

Numerical simulation of transitional flow on a wind turbine airfoil with RANS-based transition model

Zhang, Ye; Sun, Zhengzhong; van Zuijlen, Alexander; van Bussel, Gerard

DOI

[10.1080/14685248.2017.1334908](https://doi.org/10.1080/14685248.2017.1334908)

Publication date

2017

Document Version

Final published version

Published in

Journal of Turbulence

Citation (APA)

Zhang, Y., Sun, Z., van Zuijlen, A., & van Bussel, G. (2017). Numerical simulation of transitional flow on a wind turbine airfoil with RANS-based transition model. *Journal of Turbulence*, 18(9), 879-898. <https://doi.org/10.1080/14685248.2017.1334908>

Important note

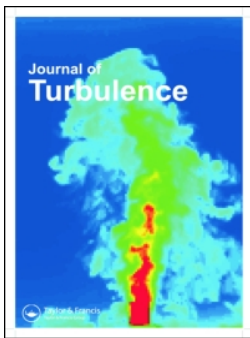
To cite this publication, please use the final published version (if applicable). Please check the document version above.

Copyright

Other than for strictly personal use, it is not permitted to download, forward or distribute the text or part of it, without the consent of the author(s) and/or copyright holder(s), unless the work is under an open content license such as Creative Commons.

Takedown policy

Please contact us and provide details if you believe this document breaches copyrights. We will remove access to the work immediately and investigate your claim.



Numerical simulation of transitional flow on a wind turbine airfoil with RANS-based transition model

Ye Zhang, Zhengzhong Sun, Alexander van Zuijlen & Gerard van Bussel

To cite this article: Ye Zhang, Zhengzhong Sun, Alexander van Zuijlen & Gerard van Bussel (2017) Numerical simulation of transitional flow on a wind turbine airfoil with RANS-based transition model, Journal of Turbulence, 18:9, 879-898, DOI: [10.1080/14685248.2017.1334908](https://doi.org/10.1080/14685248.2017.1334908)

To link to this article: <https://doi.org/10.1080/14685248.2017.1334908>



Published online: 08 Jun 2017.



Submit your article to this journal [↗](#)



Article views: 397



View related articles [↗](#)



View Crossmark data [↗](#)



Citing articles: 4 View citing articles [↗](#)



Numerical simulation of transitional flow on a wind turbine airfoil with RANS-based transition model

Ye Zhang^a, Zhengzhong Sun ^b, Alexander van Zuijlen^a and Gerard van Bussel^a

^aFaculty of Aerospace Engineering, Delft University of Technology, Delft, The Netherlands; ^bCity, University of London, London, UK

ABSTRACT

This paper presents a numerical investigation of transitional flow on the wind turbine airfoil DU91-W2-250 with chord-based Reynolds number $Re_c = 1.0 \times 10^6$. The Reynolds-averaged Navier–Stokes based transition model using laminar kinetic energy concept, namely the $k - k_L - \omega$ model, is employed to resolve the boundary layer transition. Some ambiguities for this model are discussed and it is further implemented into OpenFOAM-2.1.1. The $k - k_L - \omega$ model is first validated through the chosen wind turbine airfoil at the angle of attack (AoA) of 6.24° against wind tunnel measurement, where lift and drag coefficients, surface pressure distribution and transition location are compared. In order to reveal the transitional flow on the airfoil, the mean boundary layer profiles in three zones, namely the laminar, transitional and fully turbulent regimes, are investigated. Observation of flow at the transition location identifies the laminar separation bubble. The AoA effect on boundary layer transition over wind turbine airfoil is also studied. Increasing the AoA from -3° to 10° , the laminar separation bubble moves upstream and reduces in size, which is in close agreement with wind tunnel measurement.

ARTICLE HISTORY

Received 23 February 2017
Accepted 19 May 2017

KEYWORDS

Boundary layer transition;
laminar separation bubble;
wind turbine aerodynamics;
RANS modelling; laminar
kinetic energy

1. Introduction

At present, wind turbines are being up-scaled towards 10–20 MW in offshore wind farms. The power increase gives rise to larger rotor blades, which are apparently more costly and more flexible. Therefore, detailed flow investigations over such large blades are needed to ensure operations. One particular phenomenon that plays a key role in blade performance is the laminar–turbulent transition (LTT). The LTT is not only crucial in aerodynamic characteristics of wind turbine airfoil, but also in forming laminar separation bubble (LSB). The LSB is very sensitive to flow perturbation and it may burst during the blade rotation. Consequently, it could cause the double-stall phenomenon, which decreases the wind turbine performance significantly [1]. As a result, accurate LTT prediction is of great importance for the aerodynamic design and analysis of wind turbine blade, and it is aimed as the first objective in the present work.

Benefitting from the rapid development of flow simulation methodology, transition has been extensively investigated by computational fluid dynamics (CFD) methods. The direct

numerical simulation (DNS) and the large eddy simulation (LES) have delivered promising results in transition simulations [2,3]. However, the expensive computational hours due to high grid resolution and unsteady simulation are still deterring their widespread application. On the other hand, the Reynolds-averaged Navier–Stokes (RANS)-based turbulent flow modelling is still the workhorse in the aerodynamic-related simulations, as it is able to provide reasonably good results for attached flow and flow with minor separation under small or moderate requirements of computation resources. Therefore, it would be very useful to accurately predict transitional flow using RANS models. One of the most widely adopted approaches [4] for transition prediction in general-purpose CFD methods is the concept of intermittency, which is used to blend together laminar and turbulent flow regimes. The transport equation of the intermittency factor γ is numerically solved to predict transition. The main drawback of this approach is that it needs non-local information, for example, the integral thickness of the boundary layer and the state of flow beyond boundary layer [5]. The intermittency concept in transition prediction has been further improved by Menter et al. [6] in order to eliminate the non-local information. An additional transport equation of the transition-onset Reynolds number Re_{θ_t} , a function of the boundary layer momentum thickness, is formulated. This model shows very promising prediction for two-dimensional (2D) and 3D configurations, but the empirical correlations used in this model are proprietary [7]. A complete review on RANS-based transition modelling can be found in several articles [5,8,9]. The present introduction does not aim to provide a thorough review of all the relevant methods for transition simulation. Instead, emphasis is placed on the recently proposed RANS-based transition model using the laminar kinetic energy (k_L) concept, namely the $k - k_L - \omega$ transition model, which enables transition modelling without any empirical input or pre-knowledge of the flow.

The concept of laminar kinetic energy in boundary layer transition was originally proposed by Mayle [10] to address the transition-induced aerodynamic and heat transfer problems in gas turbine engines. But, the original model containing k_L is not a single-point model and requires pre-knowledge of the flow field. The true single-point transition model using laminar kinetic energy was actually proposed later by Walters and Leylek [11], and it contains three transport equations for turbulent kinetic energy, laminar kinetic energy (k_L) and turbulent dissipation (ϵ), namely the $k - k_L - \epsilon$ transition model. The equation of turbulent dissipation was shortly replaced by that of specific dissipation rate (ω) by Walters and Leylek [12] and becomes the $k - k_L - \omega$ transition model. The $k - k_L - \omega$ model was later improved by Walters and Cokljat [13] in order to include shear-sheltering concept as transition initiation. The Walters–Cokljat $k - k_L - \omega$ model receives attention quickly and was validated with transitional flat plate test cases by Fürst [14], who states that there are some errors or probable typos for the $k - k_L - \omega$ model in the original paper [13].

The Walters–Cokljat $k - k_L - \omega$ model has been evaluated through several types of flow. In the flat plate transition cases, comparison was carried out against the ERCOFTAC T3 database [13–15], where several free-stream turbulence levels and pressure gradients are concerned. Since the model was originally proposed to address transition-induced heat transfer problem, transition in cascade was also validated in gas turbine applications [11,13,16–18]. Transition on the aerospatiale airfoil is the third flow type for validation. LSB was claimed to be present at the transition location [19]; however, no detailed analysis of transition process and the LSB were provided. Therefore, the second objective of the

present work is to perform a detailed analysis of the transitional flow over the wind turbine airfoil.

Different from airfoils in gas turbine and aeronautical applications, wind turbine-dedicated airfoils have distinctive features, such as much larger thickness in the inboard part of the blade. However, wind turbine airfoils have not been extensively simulated through this transition model. The transition cases that are publicly available are summarised in Table 1, where the free-stream turbulence levels and the flow Reynolds numbers are also included. Figure 1 illustrates the range of turbulent intensity and Reynolds number for all the listed simulations. In the present paper, the investigation of transitional flow over wind turbine airfoil under the condition of $Re_c = 1.0 \times 10^6$ and $Tu = 0.06\%$ extends the current knowledge in this area.

To summarise, the present work envisages to carry out transition simulation using the $k - k_L - \omega$ model for the DU91-W2-250 wind turbine airfoil with chord-based Reynolds number of 1.0×10^6 , and to investigate the LSB on airfoil surface and its response for different angles of attack. The DU91-W2-250 airfoil is chosen because an extensive wind tunnel measurement database is available, allowing comparison of surface pressure distribution, coefficients of lift and drag, and the transition location. The open-source CFD package OpenFOAM is used as flow solver. The paper is organised as follows: the $k - k_L - \omega$ transition model is first briefly introduced, followed by the numerical aspects including flow domain discretisation and grid convergence study. In Section 3, the airfoil model is validated at angle of attack (AoA) of 6.24° . The AoA is afterwards varied in the range of -3° to 10° so as to reveal the change of LSB. Conclusions are finally drawn from the observations and analysis of the resolved transition flow.

2. Methodology

2.1. Laminar kinetic energy and effective turbulent length scale

In the framework of $k - k_L - \omega$ transition model, the streamwise velocity fluctuation component u' accounts for nearly entire fluctuations of kinetic energy in the laminar region. It is thus named the laminar kinetic energy k_L by Mayle and Schulz [10]. The growth of k_L is explained through the ‘splat mechanism’ by Volino [21], in which the negative wall-normal fluctuation component v' in free-stream eddies entrains high-momentum fluid from the outer region closer to the wall and this momentum transfer results in the streamwise fluctuation component u' . The ‘splat mechanism’ illustrated by Walters and Leylek [12] is shown in Figure 2. The turbulent energy spectrum is divided into large-scale eddies and small-scale ones. The former initiates ‘splat’ and gives rise to laminar kinetic energy, whereas the latter generates typical turbulence. In order to cut off the eddy size in the $k - k_L - \omega$ transition model, an effective turbulent length scale λ_{eff} is used.

2.2. The $k - k_L - \omega$ transition model

The present $k - k_L - \omega$ transition model is based on the low-Re $k - \omega$ shear stress transport (SST) eddy viscosity model. Different from the other RANS-based transition models, such as $\gamma - Re_\theta - SST$, the advantage of the present model is the elimination of intermittency factor, which is a semi-empirical parameter that bridges the pre-transitional and

Table 1. Summary of boundary layer transition cases with $k - k_L - \omega$ model addressed in the literature.

	Transition cases	Tu	Re	
Walters and Leylek [11]	ZPG flat plate	0.02%	3,500,000	
		0.2%	3,500,000	
		2.6%	2,000,000	
	Turbine cascade	6.2%	2,000,000	
		0.6%	230,000	
		10%	230,000	
19.5%		230,000		
Walters and Leylek [12]	Highly loaded compressor-like flat plate	1.2%		
		6.4%		
Walters and Cokljat [13]	ZPG flat plate ERCOFTAC T3A-	0.87%	2,500,000	
		T3A	3.3%	1,000,000
		T3B	6.5%	1,000,000
	ZPG flat plate ERCOFTAC T3C2	T3C3	3.0%	520,000
		T3C3	3.0%	400,000
		T3C4	3.0%	180,000
		T3C5	4.0%	800,000
		VPI cascade	10%	23,000
			19.5%	23,000
	VKI cascade		0.8%	1,000,000
			4.0%	1,000,000
			6.0%	1,000,000
			1.0%	500,000
		4.0%	500,000	
		4.0%	500,000	
Sanders et al. [16,17]	A-airfoil $AoA = 13.3^\circ$	0.2%	2,000,000	
	S809 airfoil 0-20 degree	0.2%	2,000,000	
	Lightly loaded turbine blade		0.75%	100,000
			1%	100,000
			1.5%	100,000
	Highly loaded turbine blade		1%	100,000
			0.6%	25,000
		0.6%	50,000	
		0.6%	100,000	
Clare Turner [15]	ZPG flat plate			
	Valeo-CD airfoil	—*	160,000	
Furst [14]	ZPG flat plate ERCOFTAC T3A-	0.91%	3,000,000	
		T3A	3.3%	3,000,000
		T3B	9.43%	3,000,000
		T3C2	3.5%	2,000,000
Pacciani et al. [18]	T106C low speed	0.4%	50,000	
			70,000	
			90,000	
			120,000	
			150,000	
			210,000	
	T106C low speed	4%	50,000	
			70,000	
			90,000	
			120,000	
			150,000	
			210,000	
	T106C high speed	0.8%	1.2×10^5	
		2.5×10^5		
		0.7×10^5		
T108 high speed	1%	0.7×10^5		
		2.0×10^5		
Medina and Early [20]	Flat plate	0.035%	4×10^5	
		0.8%	4×10^6	
			4×10^6	
Accordi & de Lemos (2015)[19]	Backward-facing step	0.2%	4×10^6	
	A-airfoil	0.2%	2.1×10^6	

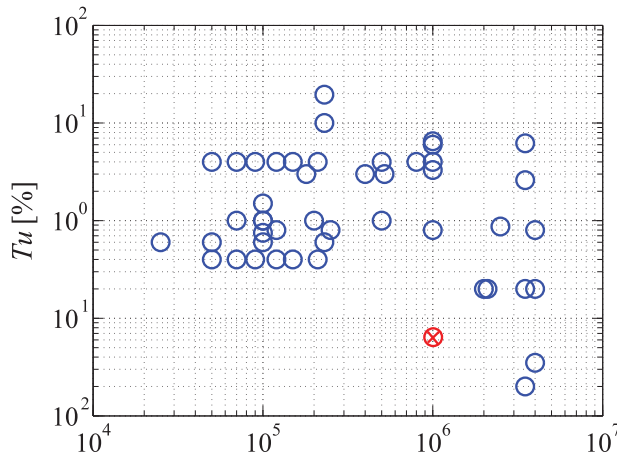


Figure 1. Turbulence intensity and Reynolds number in the summarised transition simulations using $k - k_L - \omega$ model.

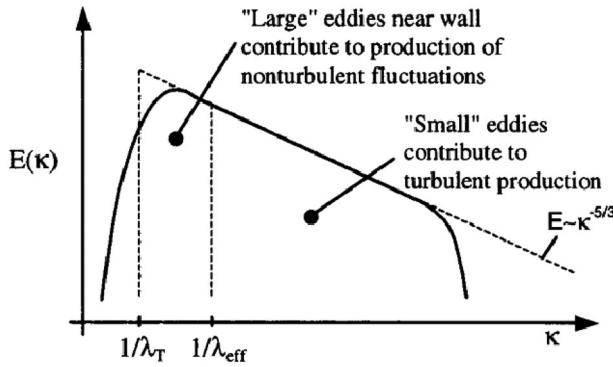


Figure 2. The ‘splat mechanism’ for production of laminar kinetic energy [12].

turbulent boundary layer and enforces transition onset [11]. The $k - k_L - \omega$ model is a three-equation model, the transport equation of k_L is added to model the low-frequency velocity fluctuations. The transport equations for the turbulent kinetic energy k_T , the laminar kinetic energy k_L and the specific dissipation rate ω in incompressible form are represented as follows:

$$\frac{Dk_T}{Dt} = \underbrace{P_{k_T}}_{\text{production}} + \underbrace{R_{BP} + R_{NAT}}_{\text{bypass and natural transition}} - \underbrace{\omega k_T}_{\text{destruction}} - \underbrace{D_T}_{\text{anisotropic dissipation}} + \underbrace{\frac{\partial}{\partial x_j} \left[\left(\nu + \frac{\alpha_T}{\sigma_k} \right) \frac{\partial k_T}{\partial x_j} \right]}_{\text{diffusion}} \tag{1}$$

$$\frac{Dk_L}{Dt} = \underbrace{P_{k_L}}_{\text{production}} - \underbrace{R_{BP} - R_{NAT}}_{\text{bypass and natural transition}} - \underbrace{D_L}_{\text{anisotropic dissipation}} + \underbrace{\frac{\partial}{\partial x_j} \left(\nu \frac{\partial k_L}{\partial x_j} \right)}_{\text{diffusion}} \tag{2}$$

$$\begin{aligned}
 \frac{D\omega}{Dt} = & \underbrace{C_{\omega 1} \frac{\omega}{k_T} P_{k_T}}_{\text{production}} + \underbrace{\left(\frac{C_{\omega R}}{f_W} - 1 \right) \frac{\omega}{k_T} (R_{BP} + R_{NAT})}_{\text{bypass and natural transition}} - \underbrace{C_{\omega 2} f_W^2 \omega^2}_{\text{destruction}} \\
 & + \underbrace{C_{\omega 3} f_{\omega} \alpha_T f_W^2 \frac{\sqrt{k_T}}{d^3}}_{\text{boundary layer wake correction}} + \underbrace{\frac{\partial}{\partial x_j} \left[\left(\nu + \frac{\alpha_T}{\sigma_{\omega}} \right) \frac{\partial \omega}{\partial x_j} \right]}_{\text{diffusion}}
 \end{aligned} \tag{3}$$

Note that the turbulent kinetic energy k_T is produced by the small-scale eddy and can be modelled through the main strain as $P_{k_T} = \nu_{T,s} S^2$, whereas the laminar kinetic energy k_L is produced by $P_{k_L} = \nu_{T,l} S^2$, which is assumed to be generated by large-scale near-wall fluctuations [11]. The small-scale eddy viscosity $\nu_{T,s}$ and the large-scale turbulence viscosity $\nu_{T,l}$ are defined as

$$\nu_{T,s} = f_v f_{INT} C_{\mu} \sqrt{k_{T,s}} \lambda_{\text{eff}} \tag{4}$$

$$\nu_{T,l} = \min \left\{ f_{\tau,l} C_{11} \left(\frac{\Omega \lambda_{\text{eff}}^2}{\nu} \right) \sqrt{k_{T,l}} \lambda_{\text{eff}} + \beta_{TS} C_{12} \text{Re}_{\Omega} d^2 \Omega, \frac{0.5 * (k_L + k_{T,l})}{S} \right\} \tag{5}$$

In Equation (4), the effective small-scale turbulence is calculated by

$$k_{T,s} = f_{SS} f_W k_T \tag{6}$$

where f_W is the damping function which relates the effective turbulent length scale $\lambda_{\text{eff}} = \min(C_{\lambda} d, \lambda_T)$ and the turbulent length scale $\lambda_T = \frac{\sqrt{k_T}}{\omega}$:

$$f_W = \left(\frac{\lambda_{\text{eff}}}{\lambda_T} \right)^{\frac{2}{3}} \tag{7}$$

Note that the damping function used here includes the exponent 2/3, as suggested in papers [14] and [12].

The viscous wall effect is included in the f_v term, which is

$$f_v = 1 - \exp \left(- \frac{\sqrt{\text{Re}_T}}{A_v} \right) \tag{8}$$

where the effective turbulence Reynolds number is calculated by

$$\text{Re}_T = \frac{f_W^2 k_T}{\nu \omega} \tag{9}$$

In addition, the shear-sheltering effect [22] is included in the f_{SS} term:

$$f_{SS} = \exp \left[- \left(\frac{C_{SS} \nu \Omega}{k_T} \right)^2 \right] \tag{10}$$

In order to satisfy the realisability constraint, the turbulence viscosity coefficient C_μ is following Shih [23]:

$$C_\mu = \frac{1}{A_0 + A_s(\frac{s}{\omega})} \tag{11}$$

In Equation (4), the term f_{INT} representing the intermittency effect on the turbulence production is

$$f_{INT} = \min\left(\frac{k_T}{C_{INT}k_{TOT}}, 1\right) \tag{12}$$

Note that the present expression is based on the corrected form by Fürst [14].

Regarding the large-scale turbulence viscosity in Equation (5), the relations are

$$Re_\Omega = \frac{d^2\Omega}{\nu} \tag{13}$$

$$\beta_{TS} = 1 - \exp\left[-\frac{\max(Re_\Omega - C_{TS,crit}, 0)^2}{A_{TS}}\right] \tag{14}$$

$$f_{\tau,l} = 1 - \exp\left(-C_{\tau,l}\frac{k_{T,l}}{\lambda_{eff}^2\Omega^2}\right) \tag{15}$$

The dissipation terms in Equations (1) and (2) should balance the diffusion terms in the laminar sublayer, which yields:

$$D_T = 2\nu \frac{\partial\sqrt{k_T}}{\partial x_j} \frac{\partial\sqrt{k_T}}{\partial x_j} \tag{16}$$

$$D_L = 2\nu \frac{\partial\sqrt{k_L}}{\partial x_j} \frac{\partial\sqrt{k_L}}{\partial x_j} \tag{17}$$

The bypass transition term R_{BP} and natural transition term R_{NAT} in the transport equations are modelled as

$$R_{BP} = C_R\beta_{BP}k_L\omega/f_W \tag{18}$$

$$R_{NAT} = C_{R,NAT}\beta_{NAT}k_L\Omega \tag{19}$$

where

$$\beta_{BP} = 1 - \exp\left(-\frac{\phi_{BP}}{A_{BP}}\right) \tag{20}$$

$$\phi_{BP} = \max\left[\left(\frac{k_T}{\nu\Omega} - C_{BP,crit}\right), 0\right] \tag{21}$$

Table 2. The constants in the $k - k_L - \omega$ transition model.

$A_0 = 4.04$	$C_{NT} = 0.75$	$C_{\omega 1} = 0.44$	$A_5 = 2.12$
$C_{TS, crit} = 1000$	$C_{\omega 2} = 0.92$	$A_v = 6.75$	$C_{R, NAT} = 0.02$
$C_{\omega 3} = 0.3$	$A_{BP} = 0.6$	$C_{\Pi} = 3.4 \times 10^{-6}$	$C_{\omega R} = 1.5$
$A_{NAT} = 200$	$C_{12} = 1 \times 10^{-10}$	$C_{\lambda} = 2.495$	$A_{TS} = 200$
$C_R = 0.12$	$C_{\mu, std} = 0.09$	$C_{BP, crit} = 1.2$	$C_{NAT, crit} = 1250$
$C_{\tau, l} = 4360$	$C_{NC} = 0.1$	$C_{SS} = 1.5$	$\sigma_k = 1, \sigma_{\omega} = 1.17$

$$\beta_{NAT} = 1 - \exp\left(-\frac{\phi_{NAT}}{A_{NAT}}\right) \tag{22}$$

$$\phi_{NAT} = \max\left[\left(\text{Re}_{\Omega} - \frac{C_{NAT, crit}}{f_{NAT, crit}}\right), 0\right] \tag{23}$$

$$f_{NAT, crit} = 1 - \exp\left(-C_{NC} \frac{\sqrt{k_L d}}{\nu}\right) \tag{24}$$

All the constants appeared in the model are summarised in Table 2. A thorough description of their physical meanings is available from the original paper [13] and they are also expressed in Table 3.

Table 3. Physical meaning of the quantities in the $k - k_L - \omega$ transition model.

Name	Meaning
D_L	laminar kinetic energy dissipation
D_T	turbulent kinetic energy dissipation
P_{k_L}	laminar kinetic energy production
P_{k_T}	turbulent kinetic energy production
R_{BP}	bypass transition production
R_{NAT}	natural transition production
Re_T	turbulence Reynolds number
Re_{Ω}	vorticity-based Reynolds number
S	magnitude of mean strain rate tensor
Ω	magnitude of mean rotation rate tensor
α_T	effective diffusivity for turbulent quantities
β_{BP}	bypass transition threshold function
β_{NAT}	natural transition threshold function
β_{TS}	Tollmien–Schlichting threshold function
λ_T	turbulent length scale
λ_{eff}	effective turbulent length scale
ν	molecular kinematic viscosity
$\nu_{T, l}$	turbulent kinematic viscosity of large-scale eddy
$\nu_{T, s}$	turbulent kinematic viscosity of small-scale eddy
ω	specific dissipation rate
ϕ_{BP}	model bypass transition parameter
ϕ_{NAT}	model natural transition parameter
d	wall distance
f_W	inviscid near-wall damping function
f_v	viscous damping function
f_v^{ω}	boundary-layer wake-term damping function
f_{INT}	intermittency damping function
f_{SS}	shear-sheltering damping function
$f_{\tau, l}$	time-scale damping function
k_T	turbulent kinetic energy
$k_{T, l}$	effective 'large-scale' turbulent kinetic energy
$k_{T, s}$	effective small-scale turbulent kinetic energy
k_{TOT}	total fluctuation kinetic energy, $k_T + k_L$

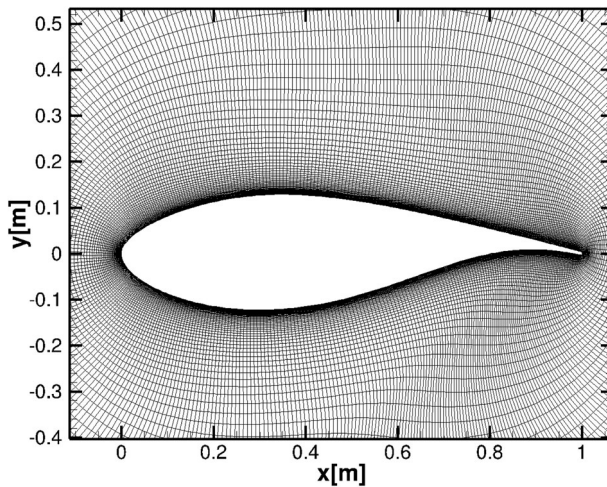


Figure 3. Grid around the DU91-W2-250 airfoil.

2.3. Case set-up and grid independence study

The wind turbine airfoil of interest is the DU91-W2-250 with $25\%c$ thickness. It is a widely used airfoil for the inboard part of commercial wind turbine blades [24,25]. The airfoil has a blunt trailing edge with thickness of $0.2\%c$. Structured O-type grid is generated around the airfoil surface, see Figure 3. The outer boundary of the simulation domain extends 100 chord length from the airfoil's aerodynamic centre ($\frac{1}{4}c$) so as to minimise the far-field boundary effect. The first wall-normal grid distance from the airfoil surface is small enough to ensure the dimensionless wall distance $y^+ < 1$, such that the viscous sublayer of the turbulent boundary layer can be resolved. The requirement of $y^+ < 1$ is essential in the use of $k - k_L - \omega$ model [13]. A stretching ratio of 1.1 for near-wall grid is applied to smoothly increase the size of the grid cells in the wall-normal direction. As transition takes place across a very short distance, the number of nodes along airfoil surface should be fine enough ($\sim 0.003c$) to capture transition and to resolve the LSB.

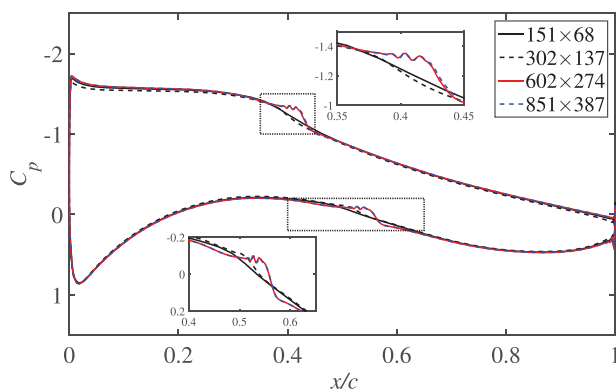
The SIMPLE algorithm [26] is used to decouple the pressure and velocity of the steady-state incompressible Navier–Stokes equations. Second-order discretisation scheme is chosen for both the convection and diffusion terms. The total variation diminishing limited linear differencing schemes with Sweby limiter are applied for velocity and turbulence quantities. All the residuals converge to a magnitude less than 10^{-4} after 10^4 iterations. Meanwhile, the lift and drag coefficients also converge. The boundary condition at the inlet is specified as Dirichlet-type condition with fixed value for the velocity and turbulent intensity, while Neumann boundary condition with zero gradient is set at the outlet boundary. A non-slip wall condition is applied at the airfoil surface. Free-stream turbulence is specified through the turbulence intensity Tu and its length scale l . In order to facilitate proper comparison with experiment, the choice of Tu follows that in the wind tunnel measurement carried out with $Tu = 0.06\%$. The turbulent length scale is estimated to be $l = 1\text{ mm}$, corresponding to the 1mm diameter of the wire mesh in the wind tunnel settling chamber. The inlet boundary condition including velocity and turbulent parameters is summarised in Table 4.

Table 4. Inlet boundary condition in the simulation.

Name	Quantity
α	6.24°
Re_c	1.0×10^6
k_T	$1.152 \times 10^{-4} \text{ m}^2/\text{s}^2$
ω^{-1}	10.73 s^{-1}
Tu	0.06%
ν_T/ν	0.73

Table 5. Grid configurations used in grid independence study.

Case	Nodes distribution	y^+	Streamwise grid spacing $100* dx/c$	Total cells
A	$151 \times 68 \times 2$	<2	0.015 ~ 2.5	20,536
B	$302 \times 137 \times 2$	<1	0.005 ~ 1.1	82,748
C	$602 \times 274 \times 2$	<0.5	0.004 ~ 0.5	329,896
D	$851 \times 387 \times 2$	<0.3	0.003 ~ 0.3	658,674

**Figure 4.** Mesh resolution study of the pressure coefficient C_p .

Four grid densities as listed in Table 5 are investigated to check grid independence as well as to examine the capability in transition identification at $Re_c = 1.0 \times 10^6$ and AoA is 6.24° . The maximum y^+ along the airfoil surface is also included in Table 5. The distributions of pressure coefficient using the four grids are shown in Figure 4. It is apparent that transition, which is represented by the kink in the C_p curve, is not captured by Grids A and B. The C_p curves from Grids C and D overlap, thus grid-independent solution is obtained by Grid C. Since the 2D computation is not so expensive, Grid D with node size of $851 \times 387 \times 2$ is adopted for the present simulations.

3. Results and discussions

In this section, simulation result at $\alpha = 6.24^\circ$ is studied comprehensively. The boundary layer transitions resulted from a range of AoAs are later investigated, aiming to reveal the effect from AoA. Finally, the effects of $k - k_L - \omega$ transition model on the integral aerodynamic characteristics, including C_L and C_D , are discussed.

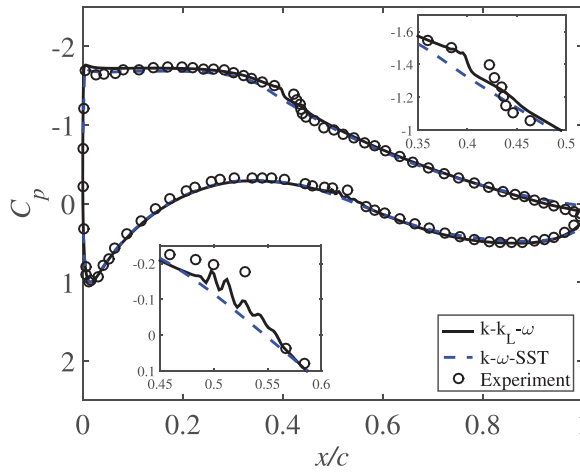


Figure 5. Pressure coefficient C_p distributions along airfoil surfaces.

3.1. Transition at $\alpha = 6.24^\circ$ with $Re = 1.0 \times 10^6$

Flow validation is first performed for the case of $\alpha = 6.24^\circ$, with $Re = 1.0 \times 10^6$ through lift and drag coefficients and pressure distribution. The transition result is also analysed in detail so as to reveal the transition process resolved by the model and the role of LSB in transition.

3.1.1. Comparison with experiment.

The wind tunnel measurement database for the DU-W2-250 airfoil allows comparison of surface pressure distribution, lift and drag coefficients, as well as transition location. The pressure distributions along the upper and lower surfaces are compared in Figure 5, where the result of $k - \omega - SST$ model is also included. Note that the simulation using $k - \omega - SST$ model is carried out with the same grid (Grid D). Both models exhibit reasonably good performance in surface pressure prediction. Since the lift coefficient is mainly determined by the pressure over airfoil, C_L for both models are within 10% difference, see Table 6.

The boundary layer transition is represented through the kink in the curve of pressure distribution returned by $k - k_L - \omega$ model at $x/c \approx 0.4$ on the suction side and $x/c \approx 0.5$ on the pressure side. The pressure undulation associated with transition is perhaps caused by the unsteady nature of the LSB, which will be discussed in Section 3.1.2. The transition locations on the upper and lower surfaces at $\alpha = 6.24^\circ$ are also listed in Table 6. Note that

Table 6. Comparison of C_l and C_d at $Re = 1.0 \times 10^6$.

	$k - k_L - \omega$	$k - \omega - SST$	Experiment
C_l	1.2362	1.1095	1.133
C_d	0.0146	0.0226	0.0121
Transition at upper surface (x/c)	0.36~0.42	-	0.43
Transition at lower surface (x/c)	0.48~0.56	-	0.53

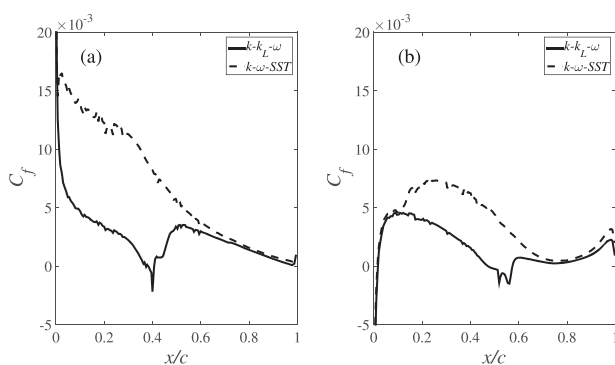


Figure 6. Skin friction coefficient C_f distributions along airfoil surface: upper surface C_f (left); lower surface C_f (right).

the transition locations in the present simulation are represented through the streamwise extension of the LSB, which is the distance between the separation point of laminar boundary layer and the reattachment point of turbulent boundary layer. It can be found that the reattachment point agrees with the wind tunnel measurement. In contrast, no such pressure kink is present in the pressure curves of $k - \omega - SST$ model, which simulates the fully turbulent boundary layer.

The drag coefficient C_D is more sensitive to LTT. Because the turbulent boundary layer produces larger friction than the laminar boundary layer, failure in transition prediction will result in significant discrepancy in C_D . Strikingly, different C_f parameters are predicted by the two models, see Figure 6. Because the $k - \omega - SST$ model is not able to model transition, larger C_f is predicted in the portion before transition on both surfaces, resulting in a drag coefficient 86% larger than that in the wind tunnel measurement. The $k - k_L - \omega$ model apparently has better accuracy in C_D , only 20% larger. The drag coefficient for both models are also compared in Table 6.

3.1.2. Transition on the airfoil

The laminar separation bubble: The negative values of C_f inside the transition region in Figure 6 suggest that flow recirculation takes place with boundary layer transition. Since the result of the $k - \omega - SST$ model is also included. The higher values of C_f before transition again suggests that transition is not resolved by the $k - \omega - SST$ model. The two transition regions containing separation bubbles on the upper and lower surfaces are enlarged in Figure 7. Both separation bubbles are in fact tiny in size. The one on the upper surface is centred at about $x/c = 0.39$ with a length of $0.06c$ and a height less than $0.001c$, while the other one on the lower surface is centred more downstream at $0.51c$ with a longer length of $0.08c$ and a smaller height of $0.0002c$.

Boundary layer evolution: Visualisation of the boundary layer evolution is useful in understanding the transition process. Three typical boundary layer profiles in laminar, transitional and turbulent stages on the upper surface are, therefore, plotted, respectively, in Figure 8. Note that the velocity magnitude U_t in the profiles is the tangential velocity component along the wall-normal direction. The turbulent boundary layer profiles predicted

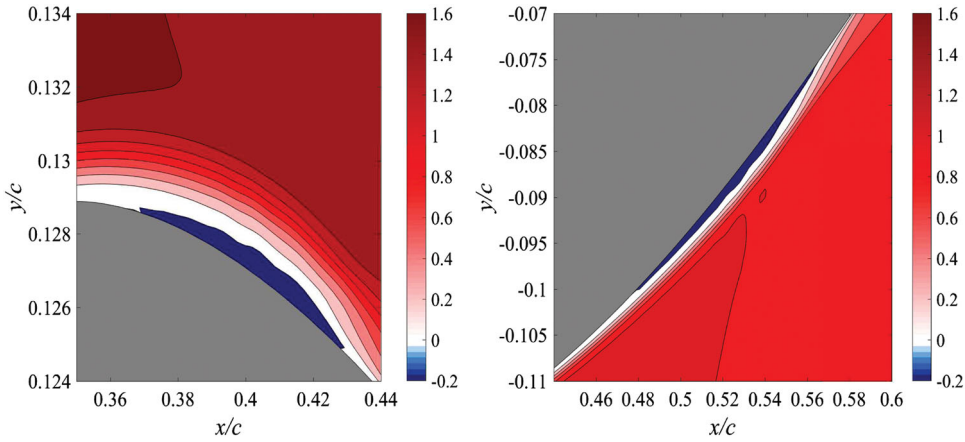


Figure 7. The contours of streamwise velocity component on the airfoil upper surface (left) and lower surface (right). The x and y scales are different to highlight the LSB.

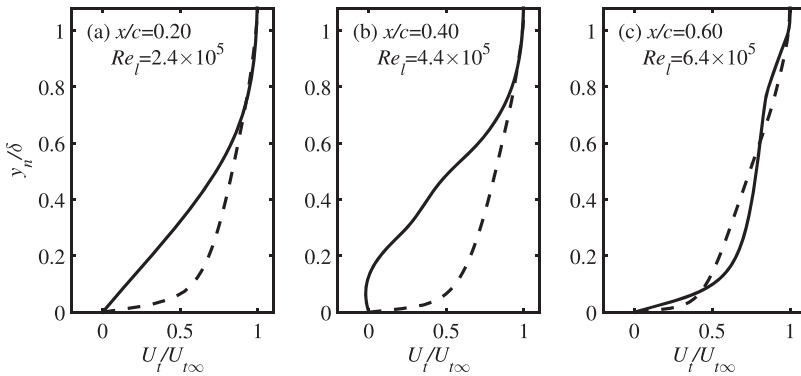


Figure 8. Boundary layer evolution along upper surface: (a) laminar; (b) transition; (c) turbulent. δ is the boundary layer thickness, which is determined by using $0.99U_{\infty}$. The solid profile (—) is the boundary layer from $k - k_L - \omega$ model, the dashed profile (- -) is the boundary layer profile from $k - \omega - SST$ model.

by the $k - \omega - SST$ model at the same locations are also included and used as a reference of turbulent boundary layer.

The boundary layer is of laminar type with thickness $\delta_{kkl} = 1.87\text{ mm}$ at $x/c = 0.20$, corresponding to a local Reynolds number $Re_l = 240,000$. The local Reynolds number is defined as $Re = \frac{U_l l}{\nu}$, where l is the surface distance between the stagnation point and the local position. This profile is less full than the turbulent one, whose thickness is $\delta_{k\omega} = 4.05\text{ mm}$.

In the transition region at $x/c = 0.40$ and $Re_l = 440,000$, velocity deficit is present due to the presence of separation bubble at the immediate vicinity of the wall. The boundary layer thickness is $\delta_{kkl} = 3.35\text{ mm}$ and $\delta_{k\omega} = 7.85\text{ mm}$ for the $k - k_L - \omega$ and $k - \omega - SST$ models, respectively. Further downstream at $x/c = 0.60$ and $Re_l = 640,000$, a typical turbulent boundary layer profile ($\delta_{kkl} = 6.43\text{ mm}$ and $\delta_{k\omega} = 14.75\text{ mm}$) is obtained. The laminar and turbulent boundary layer profiles at $x/c = 0.20$ and 0.60 , respectively, are further compared in wall unit, see Figure 9. The linear viscous sublayer at $x/c = 0.2$ extends up to

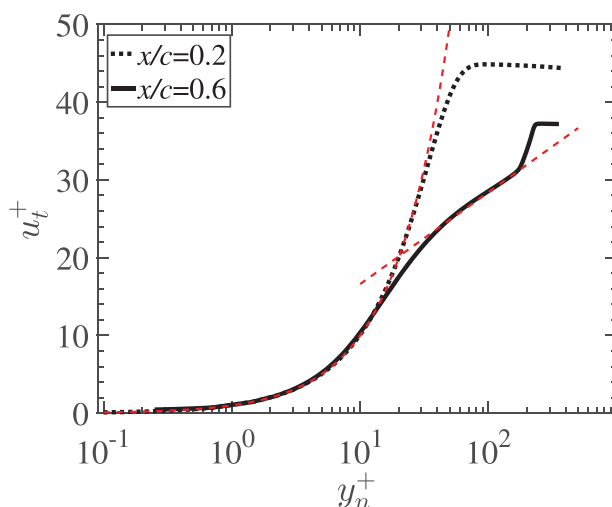


Figure 9. Laminar and turbulent boundary layers in wall unit on the upper surface predicted by $k - k_L - \omega$ model.

$y^+ \sim 30$, whereas the turbulent profile has a log portion between $y^+ = 40$ –110 and the viscous sublayer is also well resolved, which extends till $y^+ \sim 20$.

3.1.3. Laminar kinetic energy and turbulent kinetic energy

The transition process is also featured with the evolution of laminar kinetic energy and turbulent kinetic energy. According to the theory of $k - k_L - \omega$ model, k_L dominates the laminar region, where k_T should be zero. Following the onset of transition, k_T starts to increase in the transitional part, representing the generation of turbulence. Evolutions of k_L and k_T in the laminar, transitional and turbulent regions are shown in Figure 10. The magnitude of k_L increases linearly in the laminar region, while no k_T is present in this part. In the transitional region (see Figure 10(b)), k_L is subject to exponential growth, and k_T begins to appear, although its intensity is still much smaller than k_L . In the turbulent region, k_L and k_T grow initially to a maximum magnitude of $0.035U_\infty^2$ and $0.025U_\infty^2$, respectively. The intensity burst for both is later followed by a decay close to the trailing edge, see Figure 10(c). The two quantities on the lower surface have similar evolution, thus they are not shown here for conciseness.

3.2. Angle of attack effect on transition

In order to study the capability of $k - k_L - \omega$ transition model to predict the location of transitional LSB for a range of AoA. Five AoAs ranging from -3° to 10° are simulated. These AoAs are chosen in the linear regime where the RANS simulation is known to predict accurate results. The transition locations are first compared with the experiment in Figure 11. The transition location predicted by the present simulations is again represented through the start and end points of the LSB.

The airfoil model for low turbulence wind tunnel measurement is of high surface finish to ensure natural transition. According to the procedure of using microphone in the

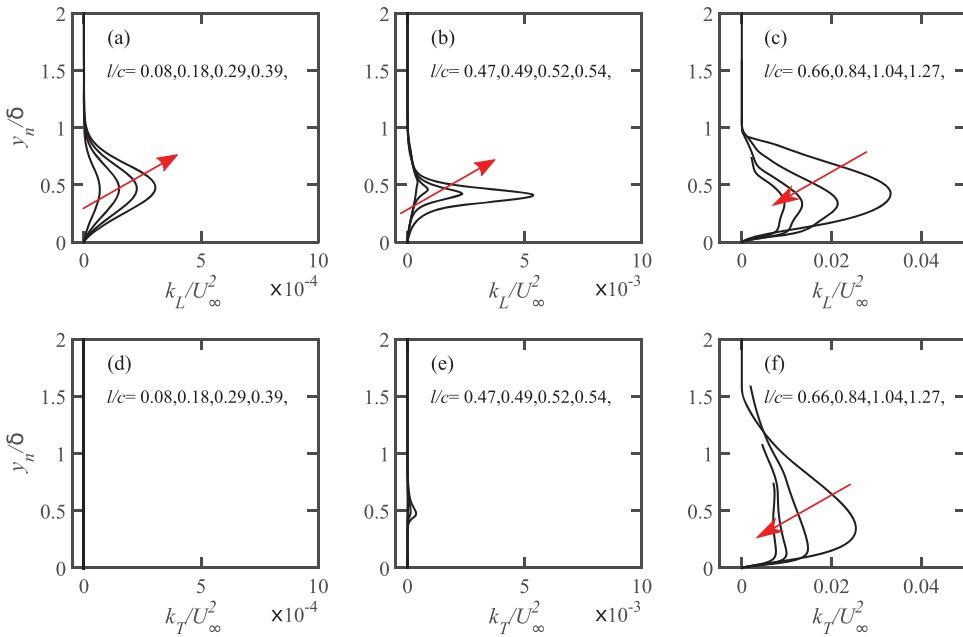


Figure 10. Evolution of laminar kinetic energy k_L and turbulent kinetic energy k_T on the upper surface in laminar region (a,d), transition region (b,e) and turbulent region (c,f). The arrow indicates the increase of l/c , where l is the arc length along the upper surface.

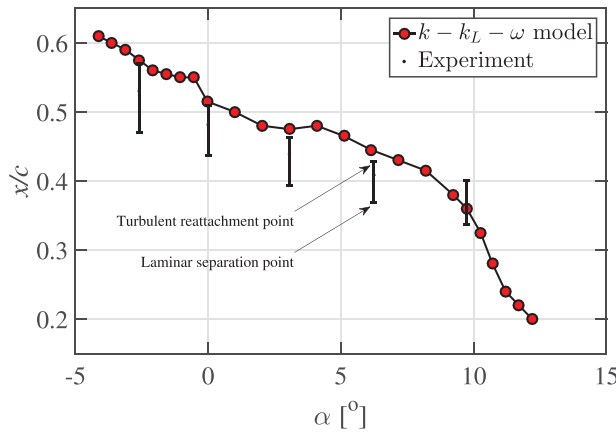


Figure 11. Comparison of transition location on the upper surface between $k - k_L - \omega$ prediction and TU Delft wind tunnel measurement.

wind tunnel measurement for transition detection, the transition location is based on the first location along airfoil where pressure fluctuation intensity is amplified. In the present simulations, the end point of the separation bubble is close to the measured transition location, although the offset grows slightly when AoA is larger than 3° . Some of the behaviours exhibited by the LSB, such as the upstream motion and the size reduction, can already be observed in Figure 11, but they will be discussed in more detail through the boundary layer velocity contours and evolution of boundary layer profiles.

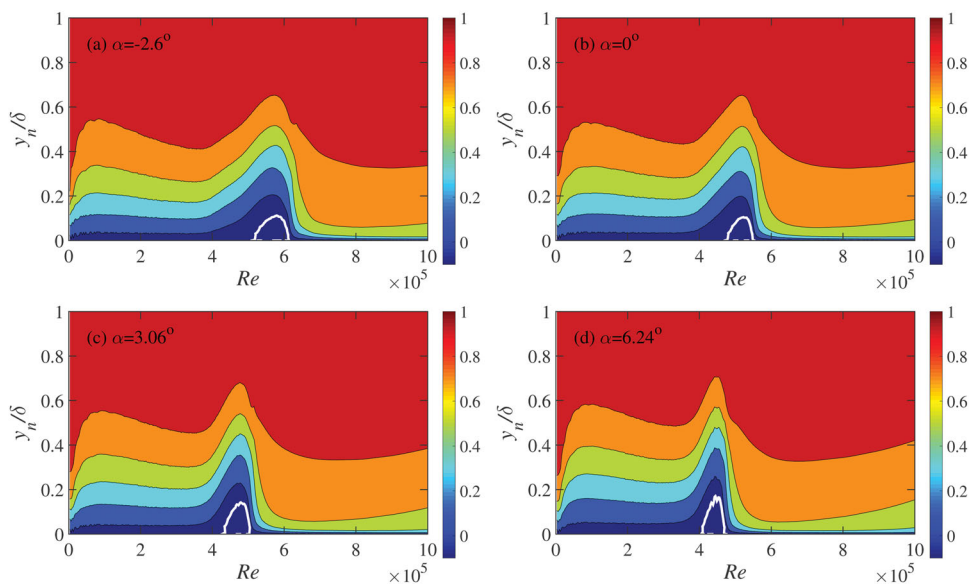


Figure 12. Contour of tangential velocity U_t/U_{t_∞} on the upper surface at different angles of attack, U_{t_∞} is the local ‘free-stream’ velocity.

The contours of tangential velocity U_t for $\alpha = -2.6^\circ$, 0° , 3.06° and 6.24° are shown in [Figure 12](#). The LSB is highlighted through the dividing contour isoline with value $U_t = 0$. In order to reveal the size of separation bubble relative to the boundary layer, the wall-normal distance is scaled with the local boundary layer thickness. The separation bubble exhibits slight growth in height: $h = 0.1\delta$ at $\alpha = -2.6^\circ$, while $h = 0.2\delta$ when $\alpha = 6.24^\circ$. The length of separation bubble becomes smaller, which means turbulent boundary layer reattaches within a shorter distance when the AoA is higher. The bubble length reduces abruptly when α increases to 9.74° , suggesting a much shorter transition process at larger AoA. Due to the tiny separation bubble at $\alpha = 9.74^\circ$, its contour plot is not shown. The corresponding Reynolds number Re_l of the start and end points of the separation bubble at the five AoAs are summarised in [Table 7](#).

The evolutions of boundary layer profile for the same AoAs are further visualised in [Figure 13](#). This type of transition visualisation provides another perspective in addition to the contour plots. The LSB is highlighted through the connection of the points where tangential velocity magnitude is zero. In the pre-transition region, all the boundary layer profiles feature the typical laminar type and the velocity gradient in the near-wall region is

Table 7. Corresponding Reynolds number of the separation bubble.

AoA	Re_l at the starting point of separation bubble	Re_r at the end point of separation bubble
-2.6°	518, 000	614, 000
0°	477, 000	551, 000
3.06°	431, 000	505, 000
6.24°	407, 000	471, 000
9.74°	365, 000	370, 000

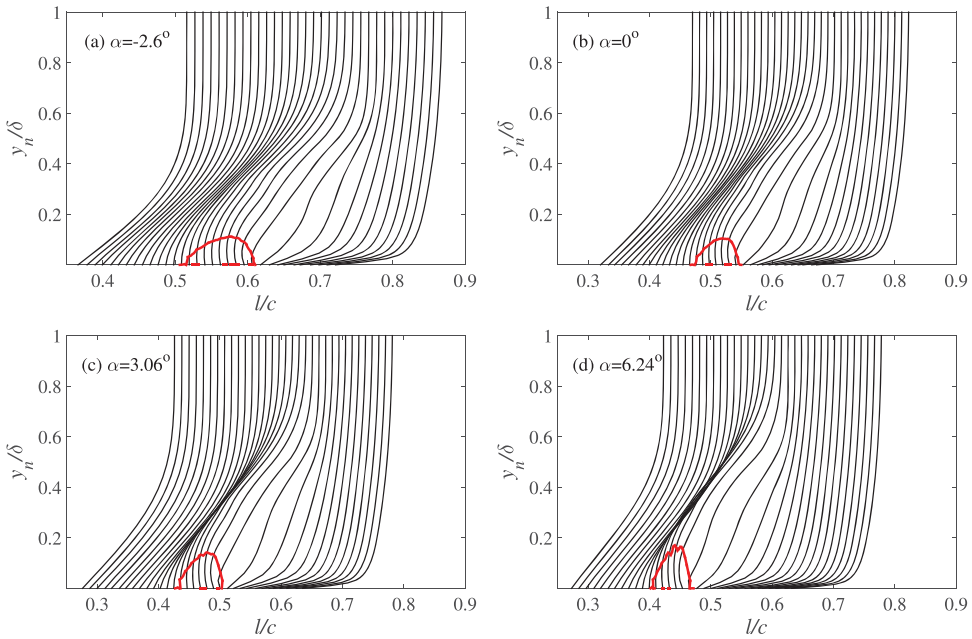


Figure 13. The evolution of boundary layers for different angles of attack. The solid line indicates the laminar separation bubble.

relatively small, which explains the smaller C_f . Once the separation bubble is produced, the transitional boundary layer deviates from the upstream laminar profile and velocity deficit can be observed right above the reversed flow. After a short recovery distance of about $0.1c$, the profile in the post-transition boundary layers features typical turbulent boundary layer.

3.3. Transition effects on airfoil polar

As shown in Section 3.1.1, the $k - k_L - \omega$ transition model delivers good results in predicting aerodynamic characteristics of the DU91-W2-250 airfoil at $\alpha = 6.24^\circ$. Significant improvement of drag force prediction has been observed from $k - k_L - \omega$ model in comparison to the $k - \omega - SST$ model. The performance of this transition model is further investigated and evaluated by extending the AOA to a wider range, namely $\alpha = -5^\circ \sim 23^\circ$. Figure 14 presents the results of airfoil drag C_D and C_L/C_D polar. In the linear regime, the drag force by the transition model $k - k_L - \omega$ is in agreement with the experiment; however, notable over-prediction is found in the results of the $k - \omega - SST$ model. This observation is consistent with the results in Section 3.1.1 for $\alpha = 6.24^\circ$, and it indicates that in the linear regime, CFD simulation with transition modelling is necessary in order to predict C_D and C_L/C_D accurately. When $\text{AoA} > 10^\circ$, due to the large trailing edge flow separation, both RANS models fail to offer good result. Delayed detached eddy simulation (DDES) is recommended for such highly separated flow.

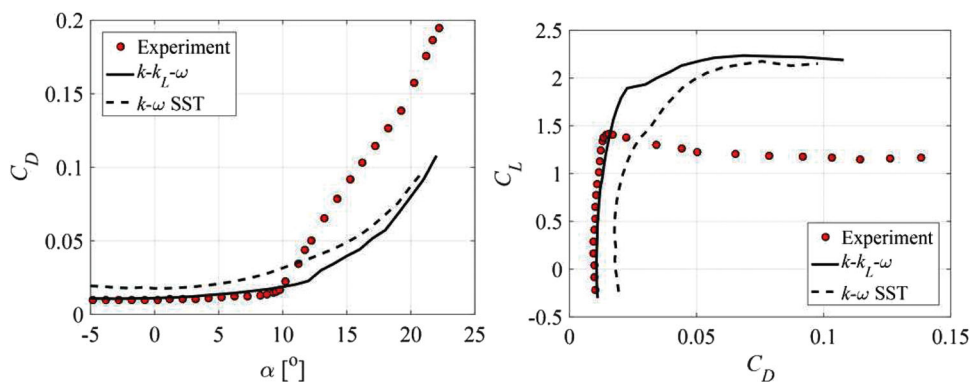


Figure 14. Transition effects on airfoil polars of C_D and C_L/C_D .

4. Conclusions

The RANS-based three-equation $k - k_L - \omega$ transition model has been successfully applied to simulate the boundary layer transition on the DU91-W2-250 wind turbine airfoil at a range of AoAs. Validation was performed for the case of $\alpha = 6.24^\circ$. Comparison with wind tunnel measurement demonstrates its accuracy in predicting transition and other quantities including pressure distribution, lift and drag coefficients. Detailed analysis of boundary layer transition at $\alpha = 6.24^\circ$ shows the LSB on both airfoil surfaces, which is closely associated with transition. The evolution of boundary layer across transition is studied by evaluating the velocity profiles at three typical stages: laminar boundary layer, transitional boundary layer and fully turbulent boundary layer. The laminar profile at $x/c = 0.2$ and the turbulent profile at $x/c = 0.6$ are well resolved in wall unit up to $y^+ \sim 30$ and $y^+ \sim 110$, respectively, by using the $k - k_L - \omega$ model. The variation of k_L and k_T across transition is present and quantitatively analysed. Investigation on the flow field at a range of AoAs clearly indicates that transition moves upstream with the increase of AoA. Regarding the accurate predictions of C_D and C_L/C_D for DU91-W2-250 airfoil in the linear regime ($-3^\circ < \text{AoA} < 10^\circ$), a transition model is required and recommended in RANS simulation. This model is inaccurate when large trailing edge separation occurs at $\text{AoA} > 10^\circ$. More advanced modelling methodology, such as DDES, is recommended for flow with massive separation.

Acknowledgements

The authors would like to acknowledge Ir. Nando Timmers from TU Delft for the discussion on the experiment. Meanwhile, the financial support of China Scholarship Council is also gratefully acknowledged. Finally, we acknowledge the OpenFOAM community and code developers.

Disclosure statement

No potential conflict of interest was reported by the authors.

Funding

China Scholarship Council

Note

1. $\omega = \text{sqrt}(k)/l$

ORCID

Zhengzhong Sun  <http://orcid.org/0000-0002-3862-7939>

References

- [1] Devinant P, Laverne T, Hureau J. Experimental study of wind-turbine airfoil aerodynamics in high turbulence. *J Wind Eng Ind Aerodynamics*. 2002;90:689–707.
- [2] Monokrousos A, Brandt L, Schlatter P, et al. DNS and LES of estimation and control of transition in boundary layers subject to free-stream turbulence. *Int J Heat Fluid Flow*. 2008;29:841–855.
- [3] Lardeau S, Leschziner M, Zaki T. Large eddy simulation of transitional separated flow over a flat plate and a compressor blade. *Flow Turbul Combust*. 2012;88:19–44.
- [4] Langtry R, Menter F. Transition modeling for general CFD applications in aeronautics. *AIAA Paper*. 2005;522:14.
- [5] Di Pasquale D, Rona A, Garrett S. A selective review of CFD transition models. *AIAA Paper* (2009-3812) (2009).
- [6] Menter F, Esch T, Kubacki S. Transition modelling based on local variables. 5th International Symposium on Turbulence Modeling and Measurements; Mallorca; 2002.
- [7] Cheng G, Nichols R, Neroorkar KD, et al. Validation and assessment of turbulence transition models. 47th AIAA Aerospace Sciences Meeting and Exhibit; 2009 No. AIAA-2009-1141; Orlando, FL.
- [8] Langtry RB. A correlation-based transition model using local variables for unstructured parallelized CFD codes [Dissertation]. Stuttgart: University of Stuttgart. 2006.
- [9] Praisner T, Clark J. Predicting transition in turbomachinery Part I: A review and new model development. *J Turbomach* 2007;129:1–13.
- [10] Mayle R, Schulz A. The path to predicting bypass transition. *J Turbomach*. 1997;119:405–411.
- [11] Walters DK, Leylek JH. A new model for boundary-layer transition using a single-point RANS approach. *J Turbomach*. 2004;126:193–202.
- [12] Walters DK, Leylek JH. Computational fluid dynamics study of wake-induced transition on a compressor-like flat plate. *J Turbomach* 2005;127:52–63.
- [13] Walters DK, Cokljat D. A three-equation eddy-viscosity model for Reynolds-averaged Navier–Stokes simulations of transitional flow. *J Fluids Eng*. 2008;130:121401.
- [14] Fürst J, Příhoda J, Straka P. Numerical simulation of transitional flows. *Computing*. 2013;95:163–182.
- [15] Turner, C. Laminar kinetic energy modelling for improved laminar-turbulent transition prediction [Dissertation]. Manchester: The University of Manchester; 2012.
- [16] Sanders DD, O’Brien WF, Sondergaard R, et al. Predicting separation and transitional flow in turbine blades at low Reynolds numbers—Part I: development of prediction methodology. *J Turbomach* 2011; 133: 031011.
- [17] Sanders DD, O’Brien WF, Sondergaard R, et al. Predicting separation and transitional flow in turbine blades at low Reynolds numbers—Part II: the application to a highly separated turbine blade cascade geometry. *J Turbomach*. 2011; 133: 031012.

- [18] Pacciani R, Marconcini M, Fadai-Ghotbi A, et al. Calculation of high-lift cascades in low pressure turbine conditions using a three-equation model. *J Turbomach.* 2011; 133: 031016.
- [19] Accordi IA, de Lemos MJ. Single-point transition modeling using the laminar kinetic energy concept. *Int J Heat Mass Transf.* 2015;89:1095–1109.
- [20] Medina H, Early J. Modelling transition due to backward-facing steps using the laminar kinetic energy concept. *Eur J Mech.* 2014;44:60–68.
- [21] Volino RJ. A new model for free-stream turbulence effects on boundary layers. *J Turbomach.* 1998;120:613–620.
- [22] Jacobs RG, Durbin PA. Shear sheltering and the continuous spectrum of the Orr–Sommerfeld equation. *Phys Fluids (1994–present).* 1998;10:2006–2011.
- [23] Shih TH, Liou WW, Shabbir A, et al. A new k-*epsilon* eddy viscosity model for high Reynolds number turbulent flows. *Comput Fluids.* 1995; 24: 227–238.
- [24] Timmer W, Van Rooij R. Summary of the Delft University wind turbine dedicated airfoils. *J Sol Energy Eng.* 2003;125:488–496.
- [25] Van Rooij R, Timmer W. Roughness sensitivity considerations for thick rotor blade airfoils. *J Sol Energy Eng.* 2003;125:468–478.
- [26] Patankar SV, Spalding DB. A calculation procedure for heat, mass and momentum transfer in three-dimensional parabolic flows. *Int J Heat Mass Transf.* 1972;15:1787–1806.